Main Chamber X-Ray Emission from the PFRC-2 Capacitively Coupled Plasma

R. Oliver,[1, a)] J. Pearcy,[1, b)] P. Jandovitz,[1, c)] C. Swanson,[1] J. Matteucci,[1] and S. A. Cohen[1]
Princeton Plasma Physics Laboratory

(Dated: 28 August 2015)

We expand upon the observation of unexpected X-ray bremsstrahlung emission from the cold, tenuous plasmas produced by a capacitively coupled RF antenna in the Princeton Field Reversed Configuration (PFRC-2) device. These X-rays, ranging in energy from 0.9 to 5keV, indicate the presence of electrons with significantly higher energies than predicted by theoretical calculations, or observed in plasmas with similar parameters. Previous work by Jandovitz et al explores properties of X-ray emission from the expansion region (ER) of the machine. We designed, calibrated, and operated a system to allow detection of X-ray emission from the main chamber (MC) of the machine using an Amptek XR-100CR X-ray detector. We report on the response of MC X-ray emission to changing plasma parameters. We observed X-ray emission from pure hydrogen (H_2), hydrogen-argon mixture, and pure argon plasmas. In all cases, X-ray emission increased with increasing power and decreased with increasing pressure. In a pure argon plasma with similar plasma parameters, X-ray emission is significantly higher, contrary to previous results in the expansion region. X-ray emission was also measured over a spatial scan in the radial direction. Potential explanations for these high-energy electrons and X-rays are being explored.

I. INTRODUCTION

The field-reversed configuration (FRC) provides a unique geometry that allows for a small high-β plasma and may one day be a viable option for producing fusion energy and propelling rockets throughout the solar system.

The PFRC-2 consists of three major regions (see Fig. 1): the main chamber (MC), the expansion region (ER), and the satellite region (SR). Surrounding these regions there are two kinds of coils: the larger outer L2 coils and the smaller innermost nozzle coils. These coils act as magnetic mirrors, confining gyrating charged particles by repulsion due to the magnetic dipoles created by the particles and the coils. There are several flux conservers on the ER: these are superconducting rings which 'compress' nearby magnetic field lines. The plasma originates in the MC and flows between the coils, where particles may either pass through or become confined by the mirrors.

A 'helicon' RF antenna capacitively couples forming a hydrogen plasma in a static magnetic field. The antenna thus 'heats' electrons. If energetic, electrons will emit X-rays while decelerating near ions and neutrals. In principle, an FRC can be generated by applying a rotating magnetic field (RMF) to this capacitively coupled seed plasma, creating an azimuthal current about the axis. The RMF generates a rotating electric field, which in turn causes a current about the axis of the plasma. This current creates a magnetic field to oppose the initial field and a separatrix forms which encapsulates a region of closed-loop magnetic field lines.

One of the central challenges the PFRC aims to tackle is to achieve a higher electron temperature. It is therefore critical to study the mechanisms that heat the plasma, as well as the resulting electron energy distributions. Measuring the spectra from X-rays emitted by the PFRC allows us to infer a great deal of information about the cause and origin of the fast electrons, which may be born from the core or on surfaces of the plasma. The combined detector system enables the study of X-rays in the ER as well as the MC, and these X-rays serve as a plasma diagnostic in those respective locations.

Another use of the fast electrons is in analysis of signals from the Langmuir probe. Because they are energetic, they will overcome the potential between the plasma and the probe at more negative voltages, resulting in a large negative probe signal. If they are produced in the capacitively coupled plasma and follow magnetic field lines tightly, then they can be used as a signature marking where this plasma follows the field. In the 'perturbation experiment' for example (Matteucci et al), the capacitively coupled plasma is pulsed with the RMF turned on, and the frequency of this pulse is picked up in the signal from the Langmuir probe when positioned at various radial distances in the plasma. Under certain conditions (odd-parity RMF), this frequency is not found in the probe signal within a certain radius, implying the magnetic field does not penetrate this radius, implying the existence of a separatrix and hence an FRC. Observing a large negative signal from the Langmuir probe produced by the fast electrons would be especially convincing, for they would only be produced during the capacitively coupled mode (so would have the same frequency) and would follow the field lines.

While expected electron energies are on the order of a few eV, previous observations by Jandovitz et al have found a small population (0.1%) of few hundred eV electrons, likely from a monoenergetic, beam-like distribu-

[a)] Brown University; Electronic mail: richard_oliver@brown.edu
[b)] Princeton University; Electronic mail: jpearcy@princeton.edu
[c)] Electronic mail: pjandovi@pppl.gov

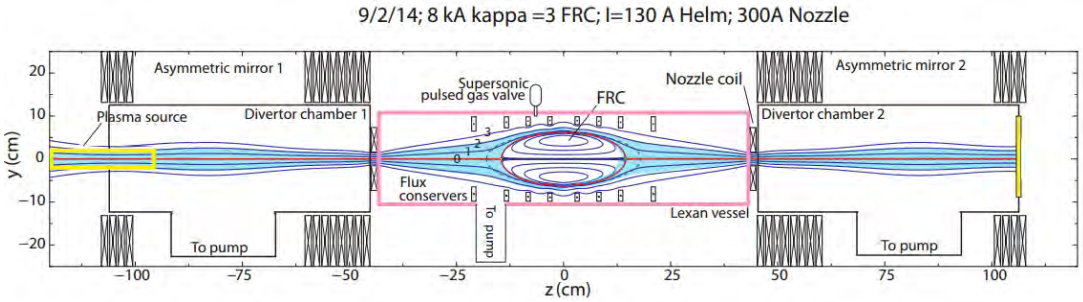

FIG. 1: A) View of the PFRC-2 in capacitively coupled mode. B) View of the PFRC-2 in field-reversed configuration.

tion. Our experiments show that these electrons are located in the core of the plasma and that the source is likely due to ion-induced secondary electron emission resulting from the floating potential on the end plate and on the Pyrex pipe comprising the source.

II. THEORY

A. Bremsstrahlung Radiation

Bremsstrahlung radiation is a form of free-electron radiation that arises from electron-ion and electron-neutral interactions. When a free electron is accelerated near another charged particle, it emits bremsstrahlung radiation. The power density below takes into account only free-free electron-ion/electron-neutral interactions. Because the plasmas in the PFRC are weakly ionized, there are far more neutrals than ions for electrons to interact with, allowing us to neglect recombination interactions. Further, the plasmas in the PFRC are not relativistic, allowing us to ignore electron-electron collisions.

For a plasma in thermal equilibrium at temperature T, corresponding to a Maxwellian electron velocity distribution, the total continuum radiation from collisions with ions and neutrals, ignoring free-bound collisions, is given by Hutchinson[1];

$$j(\nu) = n_e n_i Z^2 \left(\frac{e^2}{4\pi\varepsilon_0}\right)^3 \frac{8\pi}{3\sqrt{3}m^2c^3}\left(\frac{2m}{\pi T}\right)^{1/2} \mathrm{e}^{-h\nu/T}\bar{g}$$

Here, j is power per solid angle per unit frequency per unit volume (W s $\mathrm{sr}^{-1}\mathrm{m}^{-3}$); n_e and n_i are electron and ion densities, respectively; Z the nuclear charge; e the electron charge; m the electron mass; T the electron temperature; and $\bar{g}$ the Maxwell-distribution averaged Gaunt factor

$$\bar{g}(\nu, T) = \int_0^\infty G(\nu, E' + h\nu)\mathrm{e}^{-E'/T}\frac{dE'}{T}$$

Here, G is the dimensionless Gaunt factor, for which various approximations exist that allow us to estimate the value of $\bar{g}$ in a variety of frequency regimes. In particular, where R_y is the Rydberg energy, we have

1. The classical low frequency (Kramers) approximation;

$$\bar{g} = \frac{\sqrt{3}}{\pi}\ln\left|\left(\frac{2T}{\zeta m}\right)^{3/2}\frac{2m}{\zeta\omega}\left(\frac{4\pi\varepsilon_0}{Ze^2}\right)\right|$$

Here, ζ is the reciprocal of the Euler-Mascheroni constant γ. This approximation is valid at low frequency and $T \ll Z^2 R_y$.

2. The Born approximation, valid for $T \gg Z^2 R_y$

$$\bar{g} = \frac{\sqrt{3}}{\pi}K_0\left(\frac{h\nu}{2T}\right)\exp\left(\frac{h\nu}{2T}\right)$$

where K_0 is the modified Bessel function of the second kind. At low frequencies the Born approximation simplifies to

$$\bar{g} = \frac{\sqrt{3}}{\pi}\ln\left|\frac{4T}{\zeta h\nu}\right|$$

For a wide range of temperatures and frequencies, the Gaunt factor itself can be approximated as $G = 1$, which results in $\bar{g}$ being nearly 1 for many regimes. In this case, the temperature and frequency dependence of j is dominated by the term $T^{-1/2}\exp(-h\nu/T)$. The strong exponential dependence on temperature allows us to use bremsstrahlung spectra to measure electron temperature in the PFRC plasma.

III. EXPERIMENT

We used two Amptek XR-100CR Si-PIN X-ray detectors, one positioned at the expansion region (ER) and one at the main chamber (MC) (see Fig. 2). The detectors were calibrated using an iron-55 source.

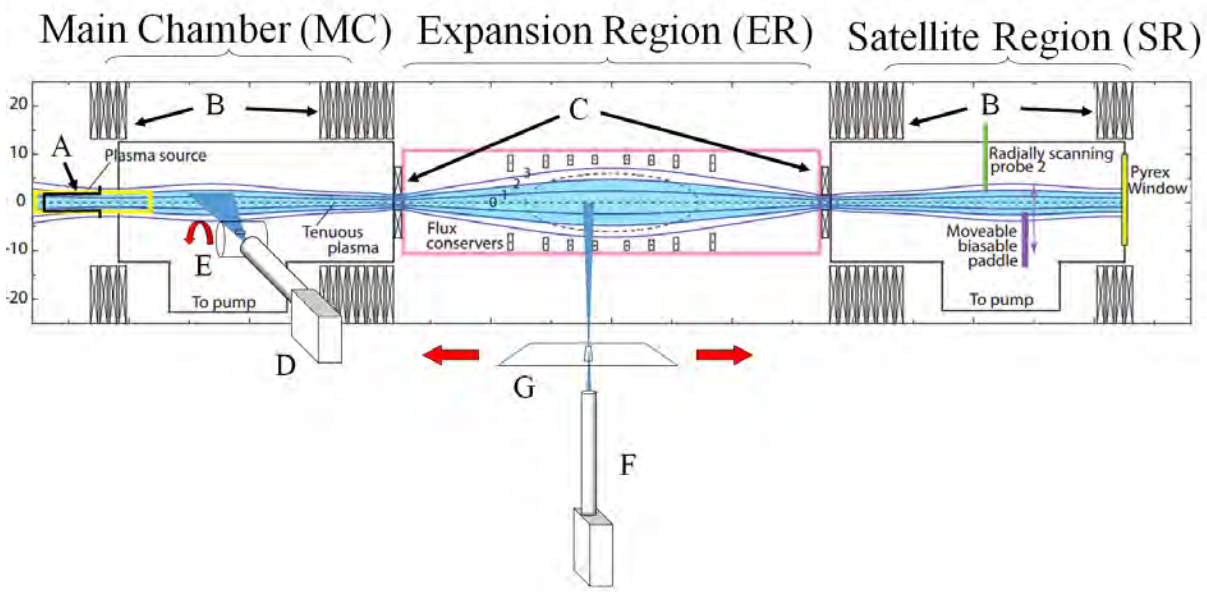

FIG. 2: (A) 'Helicon' RF antenna. (B) L2 coils. (C) Nozzle coils. (D) Main Chamber (MC) detector. (E) MC detector slit aperture. (F) Expansion Region (ER) detector. (G) ER detector slit aperture.

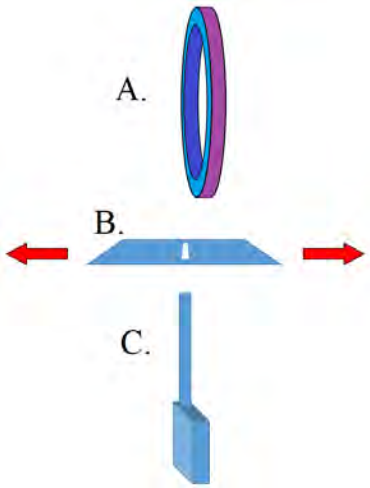

(a) The ER detector. The detector (C) looks directly upwards through the slit in the aperture at (B), which can be slid to either side of the flux conserver at (A). (Note: Figure not to scale.)

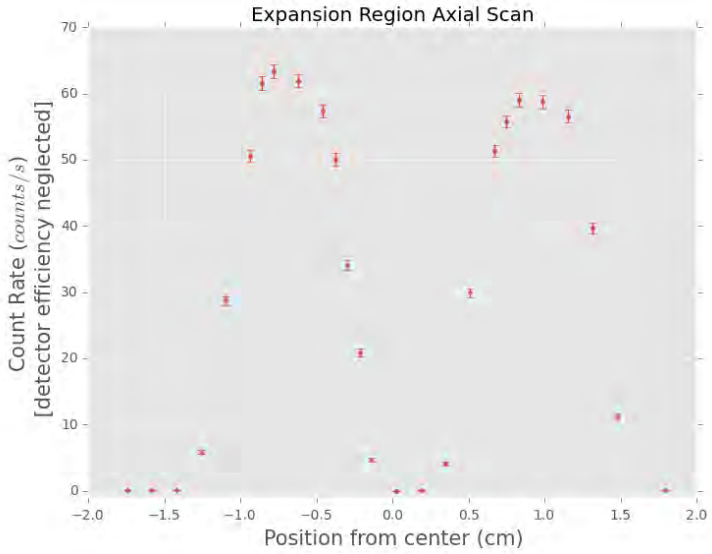

(b) An axial scan. The count rate was determined with the slit aperture at different locations along the axis of the plasma. The valley between the two central peaks is caused by the flux conserver, which blocks X-rays from reaching the detector.

FIG. 3

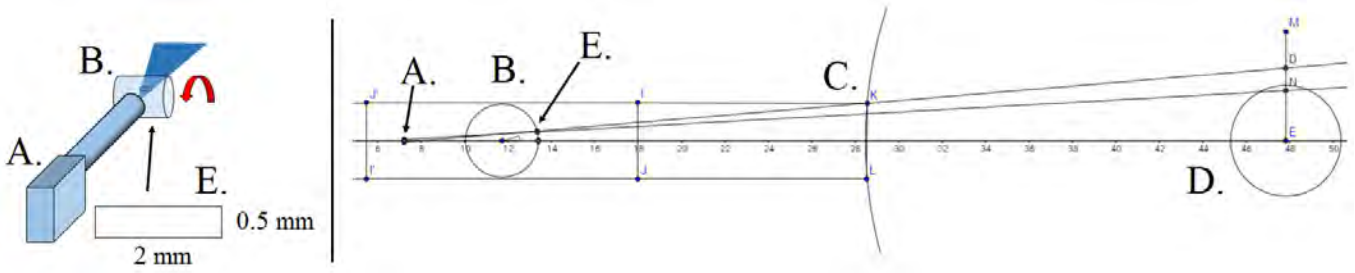

FIG. 4: The MC detector at (A) is housed in a pipe which meets the MC at (C). The slit apparatus at (B) rotates as shown in the diagram to the left, allowing the detector to vertically scan the plasma column (D), shown in approximate cross-section on the right. The slit in the aperture is shown enlarged at (E). (Note: Left fig. not to scale. Right fig. to scale in cm.)

The ER detector and corresponding slit apparatus were installed on the machine prior to our arrival in the lab. The detector itself looks straight upwards into the ER, and a sliding aperture with a slit may be placed between the detector and the plasma, shown in Fig. 3a. Taking X-ray spectra while varying the slit location along the axis of the plasma enables us to measure how the intensity of the X-rays varies along the length of the plasma column (shown in Fig. 3b). Because there is a flux conserver almost directly in the line of sight of the detector, this yields information about how intensity is affected by an obstacle.

There is a noticeable asymmetry in comparing the two peaks to the left and right of the flux conserver. This is likely attributable to the flux conserver being off-center – the detector system is located slightly to the left of the flux conserver ring. When the slit moves away from the flux conserver, count rate increases until the walls of the pipe the detector looks through come into view, blocking X-rays, and the count rate drops again. Because the flux conserver is closer to one of the pipe walls, the wall will block X-rays on this side sooner than the other, leading to the difference in peak height. If the walls were farther apart, one would expect the rates to rise to equal heights on both sides of the flux conserver before finally dropping off when the walls come into view.

The MC detector is a new addition to the PFRC-2. We designed it with the intention of scanning along the radius of the plasma column (see Fig. 4). A pipe connects the detector to the MC so that the detector may be slid to a distance of about 40-50 cm from the plasma center. At minimum distance to the plasma, the vertical resolution is 1.0 cm (the radial range ± 3.3 cm) and the horizontal resolution is 2.1 cm. At maximum extension, the vertical resolution is 0.4 cm (radial range ± 2.81 cm) with horizontal resolution 1.0 cm. Between the plasma column and the detector is a cylindrically shaped aperture with a slit which is allowed to rotate, giving the detector a range of views along the radius of the plasma column. The aperture slit is a rectangular hole 0.5×2 mm; these dimensions were chosen so as to give a reasonable resolution with as wide a total viewing range as possible. These parameters can be adjusted to a certain extent by moving the detector along the pipe.

In addition to collecting radial information about the plasma column with the slit aperture, we collected spectra while varying the electrical power to the RF antennas (in the range of 50-370 W), the current through the L2 and nozzle coils (L2 range 30-100 A; nozzle range 0-250 A), and the neutral gas pressure in the MC (range 0.5-2.0 mT). Typical values for the above parameters (when held fixed) were: RF power, 200-300 W; L2 current, 90 A; nozzle current, 200 A; MC pressure, 1.5 mT. Pressure in the ER was usually around 0.5 mT.

IV. RESULTS AND ANALYSIS

A. Radial Scan

After installing the MC detector, we performed a radial scan; we took X-ray spectra while varying the angle of the slit aperture. The data are plotted in Fig. 5. For these measurements, the detector was placed as close to the plasma as possible ($\sim$40.6 cm). Shown in the diagram are two symmetrically placed pairs of lines indicating how completely the detector's view was covered by the wall of the pipe which the detector looks through. When the aperture was rotated to angles between the lines (on either side), the wall partially blocks the field of view. At positive or negative angles beyond these lines, the field of view is completely blocked by the pipe wall.

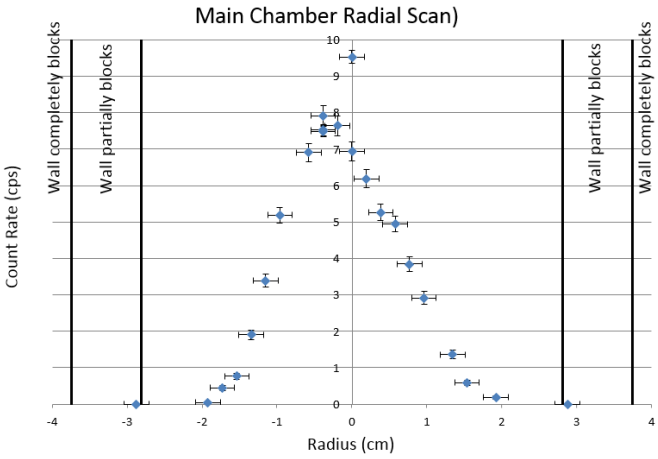

FIG. 5: By varying the angle of the slit aperture, the total count rate could be measured at different distances from the central axis of the plasma column. These angles were converted to radial distance from the plasma using the detector-plasma distance and the detector-slit distance.

The most immediate result from this data is the approximate width of the plasma column, with a total diameter of about 4 cm. One can further approximately determine the manner in which the electron temperature T_e depends on radial distance.

Similar to the axial scan results from the ER detector (Fig. 3b), there is an apparent asymmetry in the peak from the radial scan taken from the MC detector. One explanation may be found by considering that the arm attaching the detector to the MC is slightly off-center, resulting in the peak being lower than the center of the detector's field of view. If the weight of the detector and apparatus bent the arm downwards, the center of the detector's field of view would be shifted upwards, consistent with what is observed. Yet, there is a further asymmetry in the curvature on either side of the peak. While this may be attributable to the detector's being off-center, it is also possible that this asymmetry is intrinsic

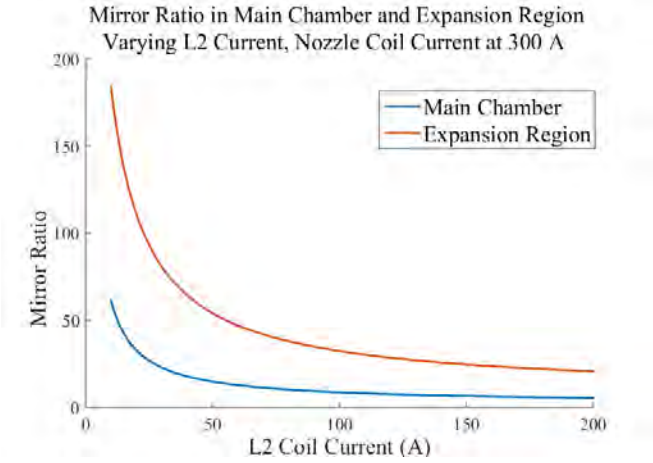

FIG. 6: A plot (made by Jackey Liu) of calculated mirror ratios in the ER and MC for typical nozzle and L2 coil currents, with the L2 coil current being varied.

to the fast electrons in the machine - axial symmetry in the fast electron population is not guaranteed.

Further analysis could be done by estimating electron temperatures from the spectra used to produce the radial scan, as outlined in the Appendix. This could yield a plot of fast electron temperature as a function of radius in the MC, and could be used to make inferences about the origin of the fast electrons.

B. The L2 and Nozzle Coils

In order to understand the manner in which the strength of the magnetic field affects the energetic electrons, the next parameters varied were the currents through the L2 and nozzle coils. In Fig. 7a there is a clear positive correlation of X-ray count with magnetic field strength generated by the L2 coils (as measured by the current).

Plots of the mirror ratios in the ER and MC were calculated for currents in the regions of interest (Fig. 6). That the mirror ratios are higher in the ER than the MC as L2 current increases suggests electrons would be more likely lost to the ER from the MC. It is therefore a surprise that the X-ray count rate increases for larger L2 currents. One plausible explanation is that as the L2 current increases it compresses the magnetic field lines in the MC (and ER). If the field lines are 'straighter' in this region, an electron's gyroradius will not be as compressed by the field and the electron will be less likely to corkscrew through the relatively small hole inside the nozzle coil. Thus the electron remains in the MC.

Another explanation is that while an electron is confined in the MC it may collide many times before being able to escape into the ER through the nozzle coil. Once this escape occurs, the electron will be more likely to escape through the second nozzle coil on the opposite side of the machine and be lost from the plasma. This process would result in fewer collisions in the ER than the MC, and fewer X-rays.

In examining the relation between count rate and nozzle coil current (Fig. 8), the correlation is not clear. Note that the points above and below the right peak were taken at lower and higher pressures, respectively, than those points in the middle (vertically).

C. RF Power

Several X-ray spectra were taken from the MC while the power to the RF helicon antenna was varied. The results are shown in Fig. 7c. It should be noted that the power as recorded is the difference between input power and reflected power; that is, not all of the power supplied to the antennas was absorbed by the plasma. While both the input and reflected power varied, only the net difference absorbed by the plasma is displayed.

The resulting plot seems to be quartic in the power; that is, it appears to show a strong correlation between the count rate and the net power raised to the fourth power.

D. Pressure

The final parameter varied was the gas pressure in the MC. This was done by taking X-ray spectra while adjusting the flow of H_2 gas into the machine. The data, shown in Fig. 7e, shows a clear negative correlation of count rate with increasing pressure.

This was perhaps one of our least expected results. According to the theory, electrons responsible for the X-rays are scattered by ions and neutrals, the latter being by far the more populous in the PFRC during the capacitively coupled mode. However, adding more neutrals to the plasma evidently decreases the amount of scattering, suggesting the added gas is interfering with the mechanism responsible for the fast electrons, although it is not clear how.

E. Argon

Some of these experiments were repeated replacing H_2 gas with Ar gas. The aforementioned parameters (magnetic field, power, pressure) were varied in the same manner as mentioned above. The dependence of average X-ray count rate on L2 coil current is shown in Fig. 7b, and appears to be consistent with the same experiment done with pure H_2 in Fig. 7a. The general trends observed with H_2 were also confirmed in experiments varying the RF power (Fig. 7d) and the pressure (Fig. 7f). Note the 4^{th} power law was also observed with Ar.

Previous results from the expansion region of the machine (Jandovitz et al) indicate that the presence of ar-

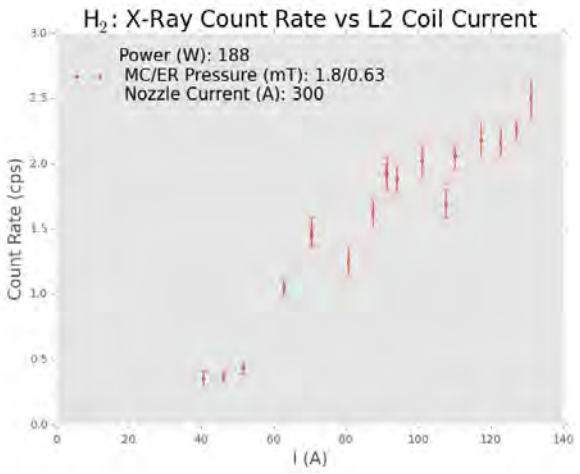
H_2: X-Ray Count Rate vs L2 Coil Current
Power (W): 188
MC/ER Pressure (mT): 1.8/0.63
Nozzle Current (A): 300
Count Rate (cps)
I (A)

(a)

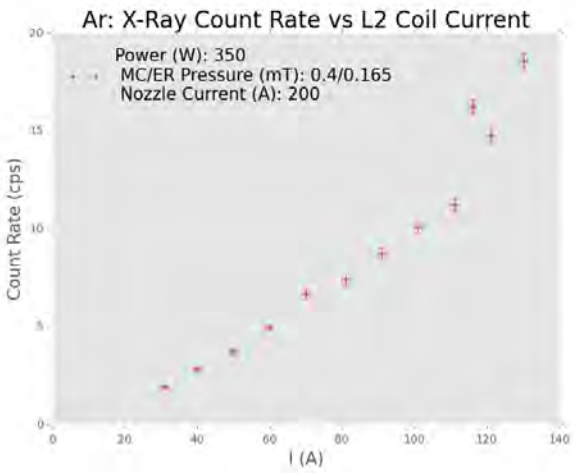
Ar: X-Ray Count Rate vs L2 Coil Current
Power (W): 350
MC/ER Pressure (mT): 0.4/0.165
Nozzle Current (A): 200
Count Rate (cps)
I (A)

(b)

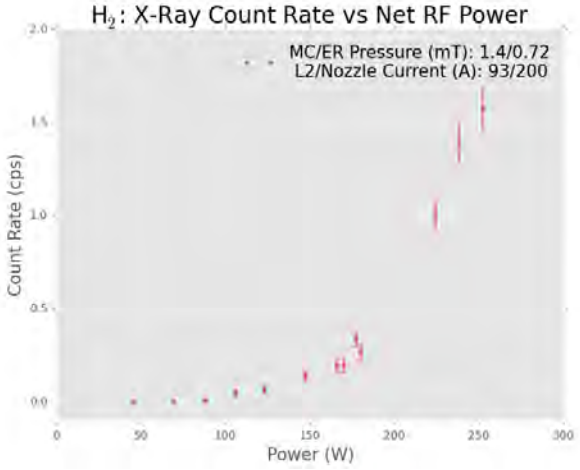
H_2: X-Ray Count Rate vs Net RF Power
MC/ER Pressure (mT): 1.4/0.72
L2/Nozzle Current (A): 93/200
Count Rate (cps)
Power (W)

(c)

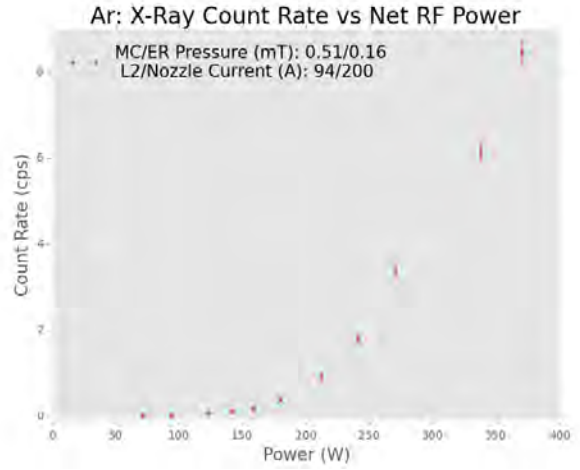
Ar: X-Ray Count Rate vs Net RF Power
MC/ER Pressure (mT): 0.51/0.16
L2/Nozzle Current (A): 94/200
Count Rate (cps)
Power (W)

(d)

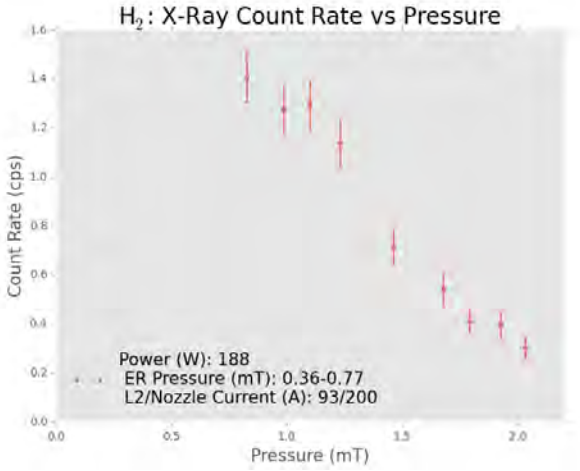
H_2: X-Ray Count Rate vs Pressure
Power (W): 188
ER Pressure (mT): 0.36-0.77
L2/Nozzle Current (A): 93/200
Count Rate (cps)
Pressure (mT)

(e)

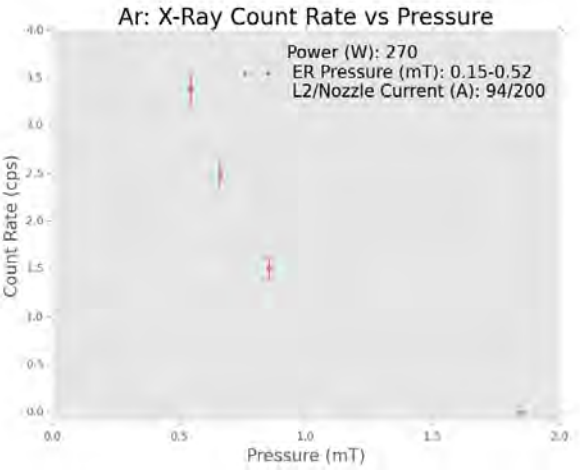
Ar: X-Ray Count Rate vs Pressure
Power (W): 270
ER Pressure (mT): 0.15-0.52
L2/Nozzle Current (A): 94/200
Count Rate (cps)
Pressure (mT)

(f)

FIG. 7

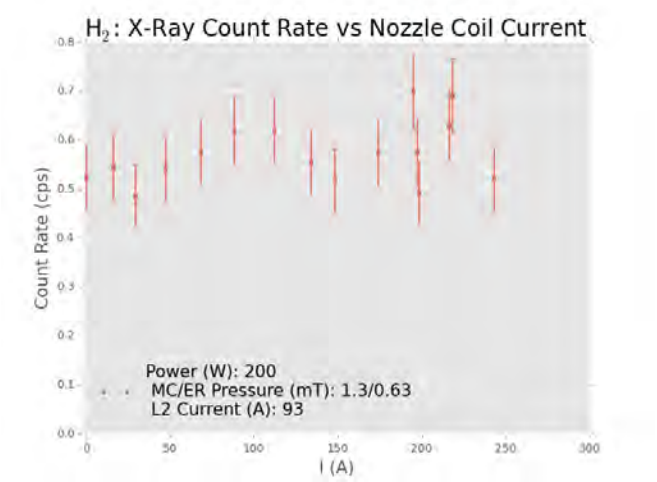

FIG. 8: X-ray count rate versus current to the nozzle coils. No significant correlation was observed.

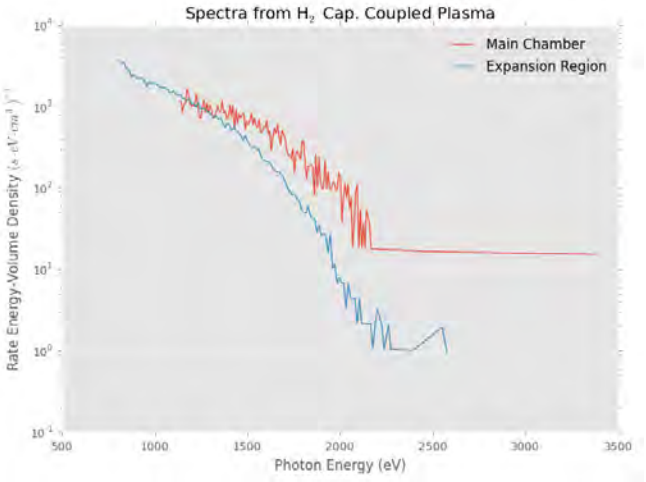

FIG. 9: Two spectra from the MC and the ER. RF Power (W): 150-160, MC/ER Pressure (mT): 1.7/0.3-0.6, L2/Nozzle Current (A): 91/300.

gon significantly reduces X-ray emission, with an 80-20 hydrogen-argon mixture displaying count rate densities six times lower than that of a pure hydrogen plasma. This trend was not observed in the main chamber, with a pure argon plasma emitting significantly more X-rays than a hydrogen plasma at similar plasma parameters.

F. Spectra Correction and Comparison

After correcting the spectra using the efficiency curves, it is necessary to find a means to compare spectra from the MC and the ER, as the two detectors have differing positions and window areas. The concept of average rate density, ρ_R, is useful to correct for this.

The rate density is defined as the number of X-rays emitted per second per unit volume of plasma. The actual X-ray count rate R is related to ρ_R and the plasma volume V as $R = \rho_R V$. Therefore, if the detector occupies a solid angle Ω, the observed X-ray count rate R_0 is given by $R_0 = \Omega R = \Omega \rho_R V$. If the distance of the detector to the plasma is r, the detector window has radius r_{det}, the radius of the plasma column is r_p, and the viewing length along the plasma axis is l, then we have (approximately) $R_0 = (\pi r_{det}^2 / 4\pi r^2)\rho_R \cdot \pi r_p^2 l$. Thus the rate density is given by:

$$\rho_R = \frac{4R_0 r^2}{\pi r_p^2 l r_{det}^2} \tag{1}$$

Every corrected raw count rate R_0 can therefore be multiplied by the factor $4r^2/\pi r_p^2 l r_{det}^2$ to find the appropriate rate density. Furthermore, this can be done to entire corrected spectra, so that for each energy bin, the count rate acquires an energy dependence. In other words, we can find for a given spectrum the rate *energy-volume* density, with units $[counts/s \cdot eV \cdot cm^3]$. In this way, entire spectra from the MC and ER can be compared on the same plot, allowing a better comparison than just looking at the net count rate for both. This has been done for two spectra taken at the same parameters (Fig. 9).

The data, once corrected, indicates an overall higher rate density in the MC than in the ER, suggesting that the fast electrons originate from the MC. One will note that the ER spectrum is 'squished' in comparison with the MC spectrum; there are fewer high-energy photons and appear to be more low-energy photons. This suggests higher-energy collisions in the MC.

Recalling that the condition for particles to be reflected by a magnetic mirror with ratio r is $\frac{v_\perp^2}{v_\parallel^2} > \frac{1}{r}$ (where $v_\perp$ and $v_\parallel$ are the velocity components perpendicular and parallel to the magnetic field, respectively), consider that for parameters in this range the MC mirror ratio is smaller than that in the ER. Therefore, electrons confined in the MC will have velocities with larger perpendicular components, and those that enter and are confined in the ER will have greater motion parallel to the field. One can infer from the spectra that there are higher-energy photons emitted from the MC. Thus, collisions that generate the higher-energy photons are more frequent when the electrons gyrate than when they translate.

V. DISCUSSION

A. Origin of the Fast Electrons

We currently have two hypotheses regarding the observation of fast electrons, both of which involve the floating potential across the sheath that forms between the end plate and the plasma. Recent measurements show that this potential oscillates at a negative voltage with amplitude slightly less than the offset. This floating potential

was measured on the order of −1 kV, comparable to the energy of the fast electrons. Furthermore, we observe that RF power correlates linearly with this average voltage V, so that X-ray count rate goes as V^4. This suggests that either 1) the floating potential causes there to be more energetic electrons, or 2) the presence of energetic electrons causes there to be a higher floating potential.

The mechanism for the first hypothesis is thought to be secondary electron emission from the end plate. Ions accelerate across the sheath through the already existing floating potential and hit the plate, freeing electrons in the collision. The electrons then accelerate the opposite direction across the sheath, entering the plasma with an energy on the order of 1 keV. The cause of the preexisting floating potential may be explained via coupling (capacitive or otherwise) with the RF antenna.

An alternative to this hypothesis begins instead with electron excitation via capacitive coupling with the RF antenna, energizing the electrons to the 1 keV range. RF rectification results in the large negative floating potential observed. The smaller mass and therefore greater agility of the electrons leads to a buildup of negative charge on the end plate, resulting in a negative DC potential on the order of the electron temperature. As the electrons in the plasma oscillate due to capacitive coupling, the floating potential oscillates at the frequency of the RF antenna. Even higher (~ -3kV) floating potentials have been measured on the Pyrex pipe enclosing the source, suggesting the helicon RF antenna is capacitively coupling with the pipe.

In favor of the first proposed explanation, a substantial (few hundred volt) floating potential has been observed on the back plate with the RF antennas on but without plasma. Thus it is plausible for the potential to arise from the antennas and accelerate electrons to higher energies. Once this is achieved, perhaps the second explanation accounts for further increase in negative potential.

B. Power Flow

It is important to consider power flow in the plasma and compare the power associated with a given electron temperature to the net power supplied to the machine.

One can find a simple relation to estimate the amount of power convected along the axis of a column of plasma. The total energy in the column at a given moment is:

$$E_{col} = uV \tag{2}$$

where V is the volume of the cylinder and u the average thermal energy density.

Supposing the plasma travels at some average speed $\langle v\rangle$, and the cylinder has cross-sectional area A and length l, the average amount of time for a particle to travel the length of the column is $t = l/\langle v\rangle$. So, the estimate for the power P becomes:

$$P = \frac{E_{col}}{t} = uA\langle v\rangle = (\alpha nkT_e)\, A\sqrt{\frac{kT_e}{m_e}} \tag{3}$$

with n the electron density, k Boltzmann's constant, T_e and m_e the electron temperature and mass. The coefficient α is written so as to account for some disagreement in the average energy of the plasma; depending on how one considers degrees of freedom, this number may be 3/2 or 5/2. A capacitively coupled plasma with parameters $n = 10^{10}$ cm^{-3}, $T_e = 4$ eV, $A = \pi(2\text{cm})^2 \approx 12.6$ cm^2, and $\alpha = 5/2$ has a convected power of 16.9 W. Even though this is an overestimate, this number is far less than the ~ 200 W typically absorbed by the plasma in capacitively coupled mode. As crude as this estimate is, this suggests convection does not account for most of the power absorbed by the plasma.

Considering power flow to the end plate of the PFRC gives a drastically different result. Stangeby[2] gives an expression for the power flux Q to a solid plate at (negative) potential Φ with respect to the plasma.

$$Q = n_{se}c_s\left[-e\Phi + 2kT_i + \frac{2kT_e e^{e\Phi/kT_e}}{\sqrt{\left(1+\frac{T_i}{T_e}\right)\left(\frac{2\pi m_e}{m_i}\right)}}\right] \tag{4}$$

where n_{se} is the electron (or ion) density at the sheath edge and $c_s = \sqrt{\frac{k(T_e+T_i)}{m_i}}$, the speed of sound in the plasma. While still only an approximate estimate, this expression gives a dependence on secondary electron emission, which may be pertinent when considering the origin of the fast electrons. We can employ the approximation given by Stangeby that $n_{se} \approx \frac{1}{2}n_0$, where n_0 is the usual plasma density (far from the sheath). Furthermore, let $\Phi = \Phi_f$, the floating potential (no bias voltage is supplied to the plate). In this case Stangeby gives[2]:

$$\Phi_f = \frac{kT_e}{e}\ln\left[\frac{\sqrt{\left(2\pi\frac{m_e}{m_i}\right)\left(1+\frac{T_i}{T_e}\right)}}{1-\gamma_e}\right] \tag{5}$$

with γ_e the secondary electron emission coefficient, the fraction of primary electron current that returns to the plasma via secondary electron emission. Substituting for n_{se}, c_s, and Φ gives:

$$Q = n_0 k\sqrt{\frac{k(T_e+T_i)}{m_i}}\left[\frac{T_e}{1-\gamma_e} + T_i - \frac{T_e}{4}\ln\frac{\left(2\pi\frac{m_e}{m_i}\right)\left(1+\frac{T_i}{T_e}\right)}{(1-\gamma_e)^2}\right]$$

Using the aforementioned parameters (including the plate surface area A) and setting $\gamma_e = 0.5$ and $T_i \approx 0$, the total power lost at one plate is $P \approx 0.48$ W. Thus, the total power lost at both plates will be roughly 1 kW, which is miniscule in comparison with the total power absorbed by the plasma. However, if we allow the secondary electron emission coefficient γ_e to vary, we find that for the given parameters if $\gamma_e > 0.98$ then $P > 100$ W. Yet, the floating potential one calculates (Eqn. 5) using high γ_e is inconsistent with the large (~ -1 kV) negative floating potential observed. It would seem that the underlying physics is more intricate than the theoretical model Stangeby provides, and further corrections may be required (as Stangeby himself states). Such corrections might include contributions from the fast electrons themselves.

C. Possible Improvements

There are several ways to improve the experiments described above. Much of the data presented could be retaken for better confirmation, and time constraints combined with shifting parameters (drifting pressure in particular) did not permit us to take as much data as we would like. Furthermore, since the machine is now equipped with two detectors, it would be ideal to take data from the MC and ER simultaneously - this would ensure the parameters were equal for both detectors at a given moment. The above spectra used to compare the plasma in the MC and ER were taken within minutes of one another, but there is room for improvement here. Finally, due to both time constraints and technical difficulties calibrations on both XR-100CR detectors were performed using only a single X-ray source (iron-55) with two emission peaks. More X-ray sources at known values could be used to perform more accurate calibrations.

D. Conclusions

Over the course of our research, we observed changes in both expansion region and main chamber X-ray emission due to variations in many plasma parameters. Although the XR-100CR detectors only give us absolute count rates, rate-density allows us to directly compare results from the two chambers despite different detector sizes and distances. Between the chambers, certain relations are consistent; higher RF power led to more X-ray emission, while higher overall pressure resulted in reduced emissions. However, the addition of argon to the system had significantly different results in the two chambers for other plasma parameters being similar: in the expansion region, the presence of even a small amount of argon reduced X-ray count rate by as much as a factor of six, with increasing argon concentration further reducing count rates; while in the main chamber, we found that even a pure argon plasma displayed X-ray count rates significantly higher than those observed in a pure hydrogen plasma. Spatial scans were performed in both regions of the PFRC; axial in the expansion region, and radial in the main chamber. The axial ER scan possibly indicates that the fast electron population is not distributed evenly, but a more detailed analysis is necessary to draw definite conclusions. The main-chamber radial scan revealed that X-ray emission is confined largely to the "obvious" plasma area, with little X-ray emission occurring in the region between the plasma and the walls of the chamber.

VI. APPENDIX

A. Determining the Temperature of a Maxwell-Boltzmann Distribution

An ideal three-dimensional Maxwell-Boltzmann distribution for a system of particles at temperature T and kinetic energy E takes the form:

$$f(E) \propto \sqrt{E} e^{-E/kT} = Q\sqrt{E} e^{-E/kT} \tag{6}$$

for Q a constant independent of E. Taking natural logarithms, one obtains:

$$\ln f(E) = -\frac{E}{kT} + \ln Q + \frac{1}{2}\ln E \tag{7}$$

The slope with respect to E is then approximated using:

$$\frac{d}{dE}\ln f(E) = -\frac{1}{kT} + \frac{1}{2E} \approx -\frac{1}{kT}$$

for $E \gg 1$.

With the assumption that for large energies the photon distribution does not deviate too drastically from the electron distribution, the slope of the observed spectra plotted on a semi-logarithmic graph will then yield the according temperature. Because of the crudeness of these assumptions, as calculated above, T serves only as a relative measure of temperature.

B. Detector Efficiency Curves

Amptek provides efficiency curves for the X-ray detectors. The curve in Fig. 10 indicates the efficiency of the detectors as a function of energy of the incident X-rays.

[1] I. H. Hutchinson. Principles of plasma diagnostics, 2nd ed. 2002.
[2] Peter C. Stangeby. The plasma sheath. In D.E. Post and R. Behrisch, editors, Physics of Plasma-Wall Interactions in Controlled Fusion, pages 41–97. Springer US, 1986.

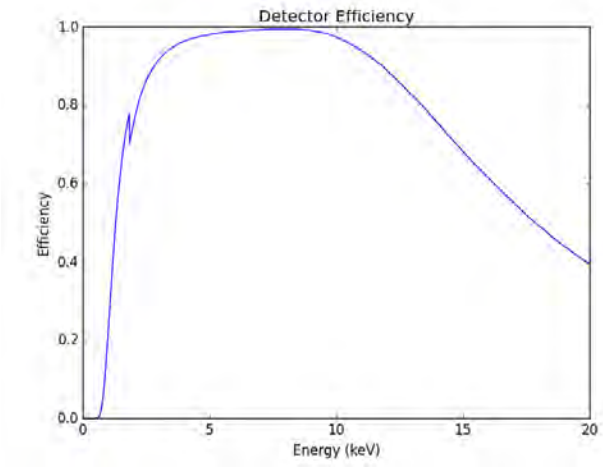

FIG. 10: X-ray detector efficiency curve.